



Spectral-divergence based pigment discrimination and mapping: A case study on *The Scream* (1893) by Edvard Munch

Hilda Deborah, Sony George & Jon Yngve Hardeberg

To cite this article: Hilda Deborah, Sony George & Jon Yngve Hardeberg (2019) Spectral-divergence based pigment discrimination and mapping: A case study on *The Scream* (1893) by Edvard Munch, *Journal of the American Institute for Conservation*, 58:1-2, 90-107, DOI: [10.1080/01971360.2018.1560756](https://doi.org/10.1080/01971360.2018.1560756)

To link to this article: <https://doi.org/10.1080/01971360.2018.1560756>



© 2019 The Author(s). Published by Informa UK Limited, trading as Taylor & Francis Group



Published online: 05 Feb 2019.



[Submit your article to this journal](#)



Article views: 406



[View related articles](#)



[View Crossmark data](#)



Citing articles: 1 [View citing articles](#)

Spectral-divergence based pigment discrimination and mapping: A case study on *The Scream* (1893) by Edvard Munch

Hilda Deborah , Sony George  and Jon Yngve Hardeberg 

Department of Computer Science, The Norwegian Colour and Visual Computing Laboratory, NTNU – Norwegian University of Science and Technology, Gjøvik, Norway

ABSTRACT

An important application of imaging spectroscopy or hyperspectral imaging is the classification or discrimination of pigments based on the obtained spectral reflectance information. As opposed to being a point-analysis tool, this non-invasive method captures the entire surface of interest. This means that its potential is not only in the discrimination of pigments but also in their mapping. However, the challenge lies in the fact that in a real painting, there is no clear-cut edge between regions with certain pure pigments or of the exact same mixture. Pigments and other paint materials mix seamlessly and continuously in the physical domain. In this article, we introduce a divergence-based approach to pigment discrimination and mapping. The methodology is then applied to Munch's masterpiece *The Scream* (1893), whose pigments and materials have been identified for several points in the painting in a previous study. Through the introduced methodology, we have been able to extend the point analyses of pigments and materials to the entire surface of the painting, recto and verso.

RÉSUMÉ

Une importante application de la spectro-imagerie ou imagerie hyperspectrale est la classification ou la différenciation de pigments en fonction des données de réflectance spectrale obtenues. Contrairement à un instrument d'analyse ponctuel, cette méthode non invasive examine la surface d'intérêt dans son ensemble. Cela signifie que son potentiel n'est pas seulement la différenciation de pigments mais aussi leur cartographie. Cependant, la difficulté réside dans le fait que dans une véritable peinture, il n'y a pas de limite nette entre des zones de pigments purs ou de différents mélanges de ces pigments. Les pigments et autres matériaux constitutifs d'une peinture se mélangent imperceptiblement et continuellement dans le domaine physique. Dans cet article nous présentons une approche basée sur la divergence de spectre pour la différenciation des pigments et leur cartographie. Cette méthodologie est ensuite appliquée au chef-d'œuvre de Munch *Le Cri* (1893), dont les pigments et matériaux constitutifs ont été identifiés en plusieurs points de la peinture dans une étude précédente. Grâce à la méthodologie proposée, nous avons pu étendre les analyses ponctuelles de pigments et autres matériaux à l'ensemble de la surface de la peinture, recto et verso. Traduit par Claire Cuyaubère.

RESUMO

Uma aplicação importante da espectroscopia de imagem ou imagem hiperespectral é a classificação ou discriminação de pigmentos com base na informação de refletância espectral obtida. Ao contrário de ser uma ferramenta de análise pontual, esse método não invasivo captura toda a superfície de interesse. Isso significa que seu potencial não está apenas na discriminação de pigmentos, mas também em seu mapeamento. No entanto, o desafio reside no fato de que, em uma pintura real, não há uma borda nítida entre regiões com certos pigmentos puros ou que contenham exatamente a mesma mistura. Pigmentos e outros materiais de pintura se misturam perfeitamente e continuamente no domínio físico. Neste artigo, introduzimos uma abordagem baseada em divergência para a discriminação e mapeamento de pigmentos. A metodologia é aplicada à obra-prima de Munch, *O Grito* (1893), cujos pigmentos e materiais foram identificados em vários pontos da pintura em um estudo anterior. Através da metodologia introduzida, pudemos estender as análises pontuais de pigmentos e materiais para toda a superfície da pintura, frente e verso. Traduzido por Marcia Rizzo.

RESUMEN

Una aplicación importante de la espectroscopia de imagen o imagen hiperespectral es la clasificación o discriminación de los pigmentos según la información de reflectancia espectral

ARTICLE HISTORY

Received 28 May 2018

Accepted 17 December 2018

KEYWORDS

Hyperspectral imaging;
spectral analysis; pigment
identification; reflectance
spectroscopy

obtenida. A diferencia de ser una herramienta de análisis puntual, este método no invasivo captura toda la superficie de interés. Esto significa que su potencial no solo está en la discriminación de los pigmentos, sino también en su mapeo. Sin embargo, el desafío radica en el hecho de que en una pintura real, no hay un borde bien definido entre las regiones con ciertos pigmentos puros o de la misma mezcla exacta. Los pigmentos y otros materiales de pintura se mezclan en forma fluida y continuamente en el dominio físico. En este artículo, presentamos un enfoque basado en la divergencia para la discriminación y el mapeo de pigmentos. La metodología se aplicó luego a la obra maestra de Munch, *The Scream* (1893), cuyos pigmentos y materiales han sido identificados en varias áreas puntuales de la pintura en un estudio anterior. Por medio de esta metodología, hemos podido extender los análisis puntuales de pigmentos y materiales a toda la superficie de la pintura, anverso y reverso. Traducido por Amparo Rueda.

1. Introduction

Hyperspectral imaging was initially developed in the remote sensing sector but later found its application in several areas, including cultural heritage digitization. With the possibility of recording high resolution in both spectral and spatial dimensions, hyperspectral images provide information of material interactions with light in different spectral regions. In turn, this results in high discrimination capabilities useful for material classification.

Pigment identification is one of the important goals of most digitization projects in the cultural heritage sector. The uniqueness of materials in terms of their physical and chemical characteristics can be used for their classification by means of reflectance spectroscopy. Despite researchers' great success on obtaining high quality spectral images, accurate pigment classification still remains a challenge. Identification and classification of pigments from hyperspectral data is a complex task due to the fact that, pigments in most of the regions in the painting are usually in mixed form and not pure pigments. There are also other issues like aging, layering, etc. Spectral unmixing techniques are supposed to help in identifying the pigments accurately. There are several unmixing techniques developed in other application areas like remote sensing, however it is difficult to apply the same in cultural heritage imaging. The main challenge lies in the different nature of mixing of the pigments that is not only optical mixing as in remote sensing applications. In many cases, there could be multiple layers of pigments superposing one another and they may mix both chemically and optically.

There have been many efforts in obtaining accurate pigment classification using spectral classification algorithms (Almeida et al. 2013; Bacci et al. 2007; Cosentino 2014; Delaney et al. 2005; Grabowski et al. 2018; Rohani et al. 2016). Chemometric techniques (Baronti et al. 1998) for classification of pigments were also investigated. However, endmembers obtained from this classification do not have any physical meaning and are not very useful in interpretation of the pigments in the painting. Pigment classification using methods based on Kubelka–Munk theory

resulted in better outcomes. However, it requires measurements of mixtures of the pigment with materials whose absorption and scattering coefficients are known. This is not the case with most paintings and, thus, limits the use of the method (Zhao 2008). Spectral Angle Mapper (SAM) (Kruse et al. 1993) is one of the commonly used similarity-based classification methods, where spectra of pure pigments forming the spectral library are compared to those in the hyperspectral image. It then classifies pigments in the painting according to their spectral match or highest similarity to entries in the library. Spectral Correlation Mapper (SCM) (de Carvalho Jr. and Meneses 2000) is an improvement of SAM, which bases its classification algorithm on correlation between spectra. It is found to be more accurate than SAM since it overcomes the limitation of SAM in detecting negative correlation (Deborah, George, and Hardeberg 2014). Nevertheless, both SAM and SCM have been shown to have limitations in its accuracy (Deborah, Richard, and Hardeberg 2015). Since then, and a new spectral difference function has been proposed and validated theoretically and metrologically, i.e., Kullback Leibler pseudo-divergence (KLPD) (Richard et al. 2016).

In this study, we present the use of a spectral-divergence based representation space for spectral variation, which is built based on KLPD, i.e., Bidimensional Histogram of Spectral Differences (BHSD) (Richard et al. 2016) and its modified version (Deborah 2016). The aim of this article is to demonstrate its applicability and relevance for pigment analysis of cultural heritage paintings, using the hyperspectral dataset of the masterpiece *The Scream* (1893) by Edvard Munch (1863–1944).

2. *The Scream* (1893), front and reverse sides

As a case study, the hyperspectral imaging-based pigment mapping will be applied to *The Scream* by Edvard Munch. Specifically, it is the painted version of *The Scream* from 1893 (tempera/ crayon/ oil, Woll 333), owned by the National Museum of Art, Architecture and Design, Oslo, Norway (Aslaksby 2015). Subsequently, the painting

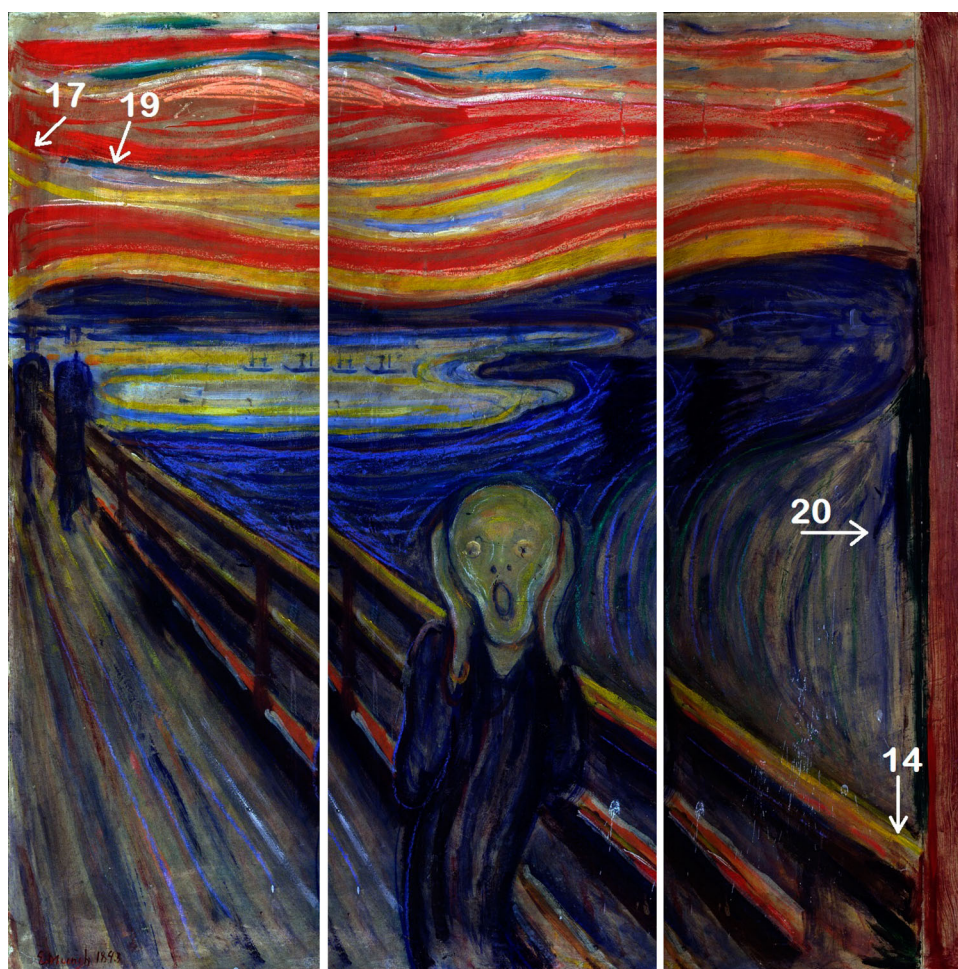


Figure 1. Three cutouts of *The Scream* (front side, 1893) as acquired by the hyperspectral scanner. The color images are generated by GLIMPS software¹ using the peak wavelengths at approximately 610, 560, and 454 nm as the RGB channels. Their brightness has been adjusted for presentation purposes. The numbers and arrows indicate the approximate location of paint samples provided in Table 1.

will be referred to as *The Scream* (1893). The painting consists of the front side and its less-known reverse side. More details of the motif of the reverse side were given by Aslaksby (2015). A hyperspectral dataset of both sides of the painting was acquired during an acquisition campaign held in 2012 (Hardeberg et al. 2015). Each side is available as three separate cutouts or hyperspectral cubes due to the acquisition setup. Color images of the cubes are shown in Figure 1 (recto) and Figure 2 (verso).

2.1. Hyperspectral image acquisition and preprocessing

Hyperspectral image acquisition has been performed using the HySpex VNIR-1600. The scanner operates in the visible and the near infrared region (VNIR) of the electromagnetic spectrum, between 0.4 and 1.0 μm . The line scanner has been used for scanning the painting at two different distances, which records high resolution and slightly lower resolution of the painting; one allowing

acquisitions at a distance of 1 m, which gives a spatial resolution of 0.2 mm, and the close-up lens with an acquisition distance of 30 cm, which provides a resolution of 0.06 mm. In order to cover the whole area of the painting, the painting has been acquired with three acquisition stripes. Each cutout shown in Figures 1 and 2 is a single hyperspectral image; sometimes also referred to as hyperspectral cube. Thus, the analysis in this study includes a total of 6 hyperspectral images. Each cube is originally of 5212×1600 pixels. They also consist of 160 channels or spectral bands from approximately 414.624–992.497 nm in about 3.634 nm intervals. However, since not all pixels are relevant for pigment mapping (e.g., they are of the wood support), each image is then spatially cropped on the edges, resulting in those shown in the two previous figures. Spectrally, we are also only processing 97 spectral bands from roughly 450–800 nm. Spectral responses obtained below 450 nm are very noisy due to the sensitivity of the sensor. As for the decision to stop at 800 nm, it is based on our observation that the



Figure 2. Three cutouts of *The Scream* (reverse side, 1893) as acquired by the hyperspectral scanner. The color images are generated the same way as Figure 1. Their brightness has been adjusted for presentation purposes.

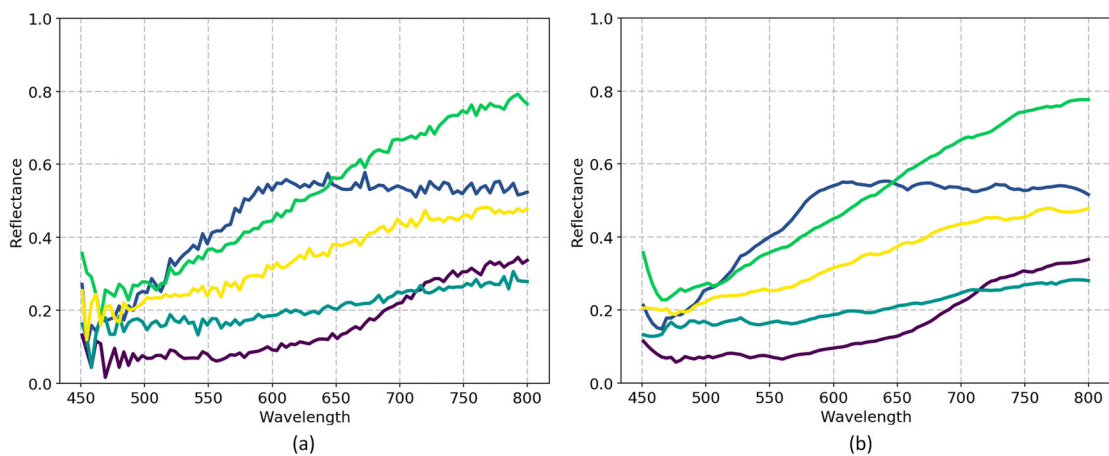


Figure 3. (a) Initial noisy spectra and (b) after they are preprocessed using Savitzky–Golay filter of window size 9 and polynomial order of 2. The filtering process acts as a smoothing filter to the noisy input.

pigments and materials we are dealing with are mainly varying in the visible range and a few nanometers into the near infrared region. Then, each hyperspectral cube is normalized to spectral reflectance, with values between 0 and 1. Finally, considering the noise level of the

reflectance spectra (Figure 3(a)), a Savitzky–Golay filter (Savitzky and Golay 1964) is employed as a smoothing filter, with parameters window size 9 and polynomial order 2. The impact this filter has on the previously shown spectra can be observed in Figure 3(b).

Table 1. Main pigments identified from paint samples of *The Scream* (front and reverse sides, 1893) (Singer et al. 2010) used in this study.

Sample number	Color, description	Main pigments
14	Yellow, lower right	Cadmium yellow and barium sulfate, vermilion, charcoal, an organic yellow containing rhamnetin, probably a buckthorn berry lake
17	Red, upper left	Vermilion and gypsum
19	Turquoise, upper left	Viridian (chromium oxide dehydrate), lead white, lead chromate
20	Blue (dark) to the right of figure	Artificial ultramarine blue, barites, clay, zinc white
33	Reverse side, red, upper left	Vermilion
34	Reverse side, blue, upper left	Ultramarine blue, lead white, barites

2.2. Spectral library of pure and mixed pigments

A prior study investigating the materials used by Edvard Munch is available (Singer et al. 2010), in which *The Scream* (1893) was also analyzed. The study provides us with its material identification carried out for 24 paint samples. The specification of several samples to be used in this study is provided in Table 1. Spatial locations where these reflectance spectra are taken from were approximately determined by the guidance of sample sites provided in reference (Singer et al. 2010). These locations can be observed in Figures 1 and 2. Note that the shown samples are not all that were identified in the previous study. They are selected for their relevance in this article.

3. Spectral variation: representation and discrimination

The notion of difference is a natural and intuitive way to measure similarity between two spectra. Given a

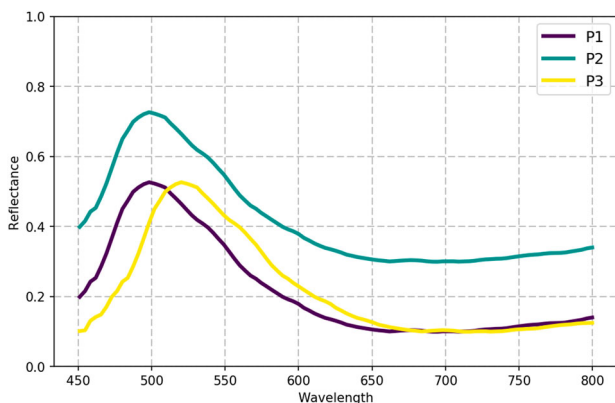


Figure 4. Three spectral reflectances to illustrate the shape and intensity components of spectral differences. P1 and P2 are considered as identical in shape (therefore zero shape difference) but different in intensity. P1 and P3 have similar intensity but different shape. P2 and P3 have both shape and intensity differences.

hyperspectral image of any arbitrary object or surface, the characteristics of this surface can be represented in terms of how different each pixel is to a pre-determined reference. This means that only a spectral difference function and a spectral reference are needed to compute such characteristics. Then, these characteristics will be useful for a discrimination task when the obtained difference measures are represented in a meaningful way, such as through the visual representation of spectral variation.

3.1. Spectral difference measure

Spectral angle, commonly known as Spectral Angle Mapper (SAM) (Kruse et al. 1993), has been widely used as the similarity measure for pigment identification or classification tasks based on hyperspectral imaging (Delaney et al. 2010; Pelagotti et al. 2008), some providing angle tolerance value of 0.4 (Daniel et al. 2016; Mounier, Denoël, and Daniel 2016). However, SAM has a drawback in its inability to detect negative correlation between two spectra. This inability can be overcome by using its so-called improvement, Spectral Correlation Mapper (SCM) (de Carvalho Jr. and Meneses 2000), which has also been confirmed in our earlier work on pigment mapping of *The Scream* (1893) (Deborah, George, and Hardeberg 2014).

Since then, there have been more fundamental studies focusing on how to accurately measure the difference between two contiguous spectra as in the case of the hyperspectral domain (Deborah, Richard, and Hardeberg 2015; Richard et al. 2016). In those studies, theoretical and metrological² limitations of both SAM and SCM and other difference measures have been extensively studied. A more suitable spectral difference function was then proposed based on information divergence, the Kullback–Leibler pseudo-divergence (KLPD) (Richard et al. 2016), whose mathematical expression is as follows

$$\text{div}_{\text{KL}}(S_1, S_2) = \Delta G(S_1, S_2) + \Delta W(S_1, S_2) \quad (1)$$

KLPD is composed of two independent components, spectral shape and intensity differences ΔG and ΔW , respectively. See formulas for both spectral differences below.

$$\Delta G(S_1, S_2) = k_1 \cdot \text{KL}(\bar{S}_1, \bar{S}_2) + k_2 \cdot \text{KL}(\bar{S}_2, \bar{S}_1)$$

$$\Delta W(S_1, S_2) = (k_1 - k_2) \log \frac{k_1}{k_2} \quad (2)$$

where Kullback–Leibler divergence function KL , normalized spectrum \bar{S} and total energy k of a spectrum S are defined by the following equations. Note that the KL function is asymmetric, thus $\text{KL}(\bar{S}_1, \bar{S}_2) \neq \text{KL}(\bar{S}_2, \bar{S}_1)$. In practice, the total energy k can be calculated through a

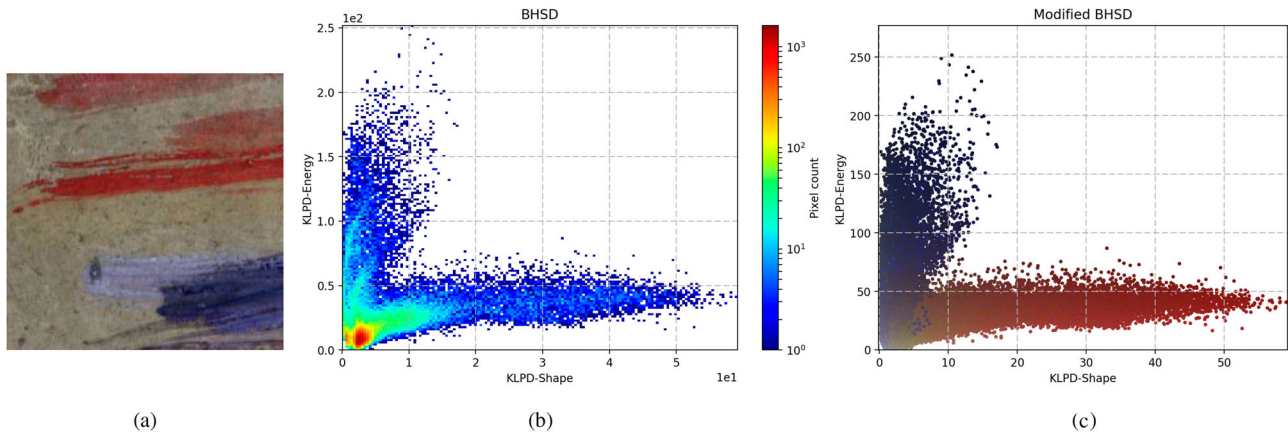


Figure 5. (a) A subset of *The Scream* (reverse side) image, shown in a color visualization. (b) Its BHS D shows the spectral distribution, providing a general idea of the number of pigment groups in the image. (c) Modified BHS D is to be read as a scatter plot, providing the actual pixel colors in addition to where it is located in the distribution.

summation operator. However, when possible, an integration function with trapezoidal rule should be used to give a calculation that is more accurate.

$$KL(\bar{S}_1, \bar{S}_2) = \int_{\lambda_{\min}}^{\lambda_{\max}} \bar{S}_1(\lambda) \cdot \log \frac{\bar{S}_1(\lambda)}{\bar{S}_2(\lambda)} d\lambda;$$

$$\bar{S} = \left\{ \bar{s}(\lambda) = \frac{s(\lambda)}{k}, \forall \lambda \in [\lambda_{\min}, \lambda_{\max}] \right\}; k = \int_{\lambda_{\min}}^{\lambda_{\max}} s(\lambda) d\lambda$$

(3)

Figure 4 is provided to illustrate what are the shape and intensity differences calculated by KLPD or other spectral difference functions. P1 and P2, both with peaks at approx. 500 nm, are considered having identical shape (therefore zero shape difference) but different intensity or energy (there is intensity displacement in the reflectance axis). P1 and P3 can be seen as having relatively similar intensity but different shape (their peaks are at approx. 500 and 460 nm, respectively). Finally, P2 and P3 are considered to have both shape and intensity differences.

Since the most important feature in pigment identification is spectral shape difference, which had initially motivated the use of SAM and then SCM, the shape component ΔG of KLPD can be used as the alternative to the two similarity measures. In Deborah et al. (2017), it was used to determine the coloring palette *Old Man in Warnemünde* (1907), another Munch painting.

3.2. Bidimensional representations of pigment distribution

Despite shape information being the most important feature in pigment discrimination tasks, intensity

differences can also provide useful information. Using the two components of KLPD allows construction of two-dimensional graphical representations of spectral differences. Bidimensional Histogram of Spectral Differences (BHS D) was introduced in Richard et al. (2016), and its modified version in Deborah (2016). In the following, a way to read and interpret them will be provided, as they will be used later in this article.

One subset of the hyperspectral image of the case study painting is shown in Figure 5(a). Using the shape ΔG and intensity ΔW components of KLPD, the distribution of all pixels in the image is plotted in a BHS D in Figure 5(b). BHS D is a histogram so every dot in it represents a frequency or pixel count. The origin of BHS D coordinate (0, 0) is the location of the spectral reference used. A spectral reference is a spectrum that is used to compute the difference functions to; its selection will be explained in more details in the following section. This means that every pixel in the image is represented in BHS D by means of its shape and intensity differences to this reference spectrum in the horizontal and vertical axes, respectively.

The BHS D in Figure 5(b) allows observer to intuitively estimate how many pigment or color groups exist in the image under observation. However, it does not provide information of which color each cluster belongs to. The modified BHS D in Figure 5(c) is provided for such complementary information. There, every dot is an individual pixel from the image represented in its true color.³ However, due to that, not every pixel can be seen in this representation since the dots overlap each other in the two-dimensional representation. Thus, this modified BHS D must be used together with the original BHS D.

By closely observing the subset image, it can be seen that there are approximately four groups of colors, i.e.,

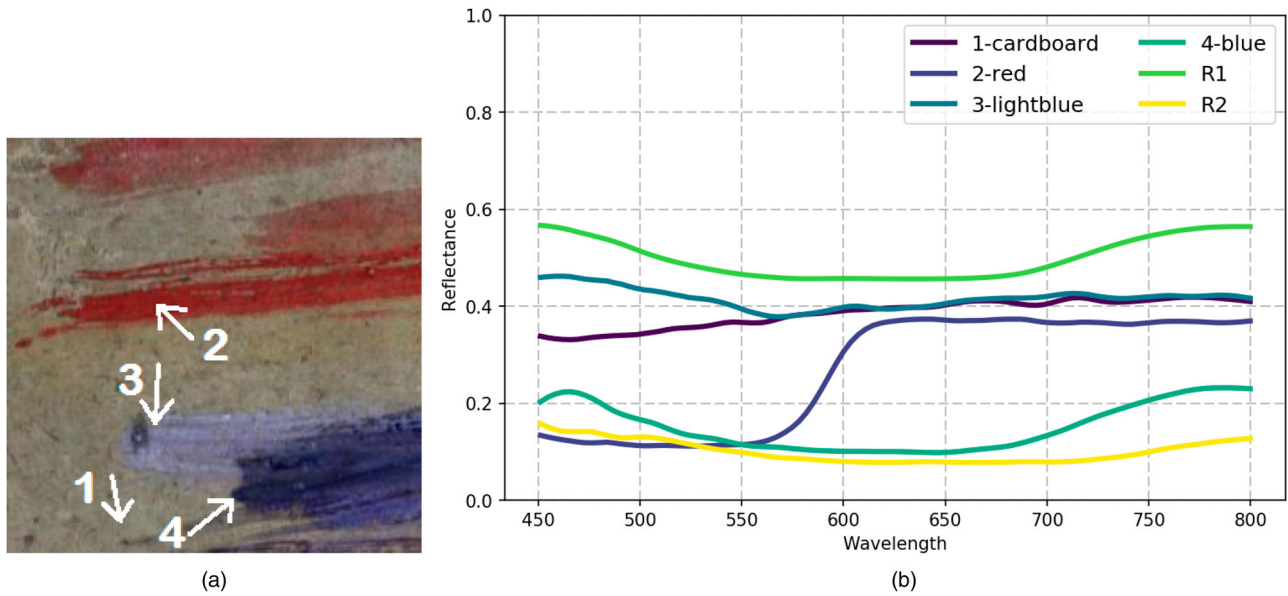


Figure 6. (a) Spatial locations of four pixels representing the four groups in the image and (b) their corresponding spectral reflectance plot. Additionally, two artificial spectra R1 and R2 are also plotted. R1 is generated to mimic a light-colored ultramarine blue pigment. R2 is created to simulate a dark greenish color.

the cardboard substrate, red, blue, and light blue. The BHSD, which plots the distribution of these colors, does not show four distinct or separate groups of clusters. Instead, there are two smaller concentrations close to the origin and two tails in both vertical and horizontal axes. Through the modified BHSD, we can observe that the two tails mainly consist of pixels with red and blue colors. Then, parts of the red tail that are closer to the origin consist of colors that progress from red to the color of the cardboard. On the other hand, the dark blue tail progresses toward the paler blue ones and, eventually, the cardboard color. This explains the two concentrations of pixels close to the origin. Through the two representations, we are able to observe the colors

or pigments distribution in a continuous manner as they mix with other colors. Also, note that in Plutino et al. (2017), BHSD representation has been compared to subjective expert judgment in pigment discrimination task. It was concluded that there is a direct relationship between expert judgment and the BHSD approach.

3.3. Selecting spectral references

The quality of pigment discrimination in a BHSD depends on how optimal the spectral reference selection is. To do so, knowledge of the image at hand as well as how BHSD works are required. To demonstrate this, the subset image previously shown in Figure 5(a) will

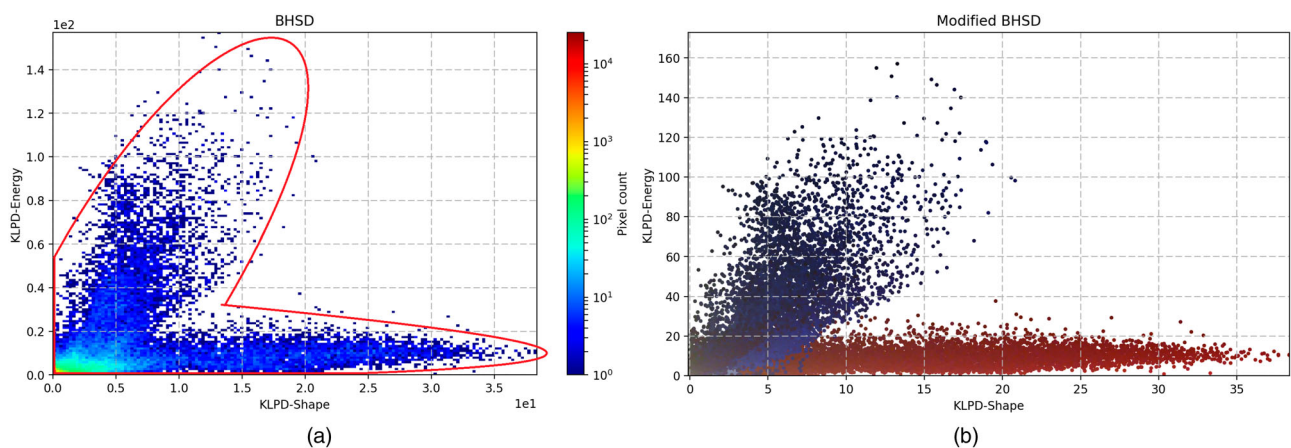


Figure 7. (a) BHSD and (b) modified BHSD of subset image shown in Figure 6(a), computed using 1-cardboard as the reference. See also spectral reflectance plot in Figure 6(b). The distribution of pixels in these BHSD representations are considered in terms of convex hull, whose outer rim is approximated by the red line in (a).

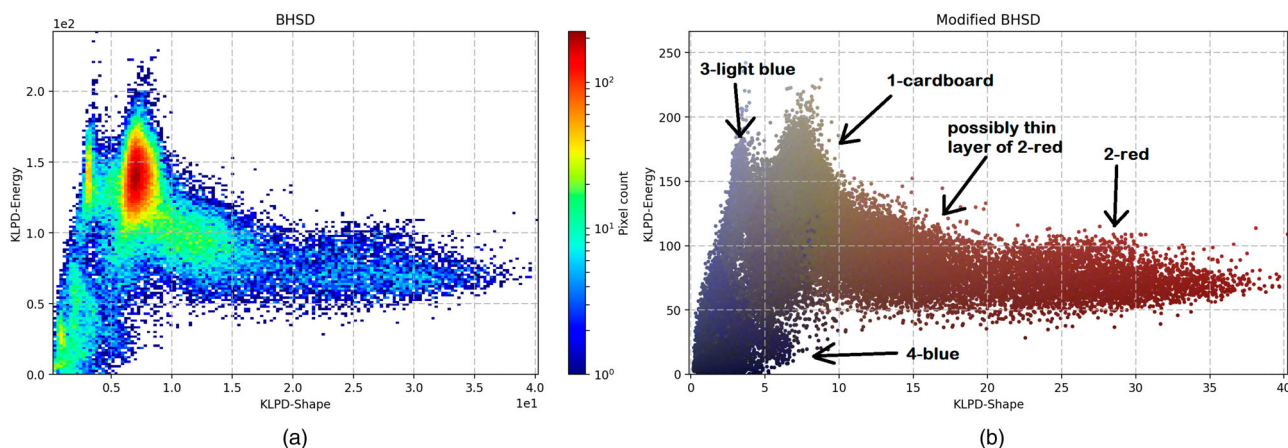


Figure 8. (a) BHS and (b) modified BHS of subset image shown in Figure 6(a), computed using R2 shown in Figure 6(b) as reference. Better pigment/ color group separation is observed, especially in the modified BHS.

be used. This subset image can be considered as consisting of approximately four color groups, the cardboard and the pigments (red, light blue, blue). Four pixels originating from these groups are selected and their reflectance spectra are plotted in Figure 6.

Distribution of spectral variations in BHS representation is considered a convex hull, see more details of the concept in Deborah (2016). Based on this, there are several criteria with which to choose the optimum spectral reference. First, the reference spectrum should not come from the initial set or image under evaluation. As an illustration, the spectrum of 1-cardboard from Figure 6(b) is employed as the spectral reference for the input image in Figure 6(a). The obtained BHS and modified BHS can be observed in Figure 7. The convex hull of this image as obtained by using 1-cardboard as reference is approximated by the region surrounded by the solid red line in Figure 7(a). Observing the obtained distribution, most pixels are concentrated around the origin and the discrimination is poor except for red pixels located far in one of the two tails of the distribution.

An optimum spectral reference should be chosen from outside the convex hull. It can be achieved by first generating an artificial spectrum whose intensity is outside the dynamic range of the dataset. To do so, we can pick any arbitrary spectrum from the initial spectral set and then modify its intensity. As an example, spectrum R1 in Figure 6(b) was generated by mimicking the shape of an ultramarine blue mixture in the painting (sample #34 in Table 1) and then shifting its intensity higher, such that it bounds or covers all other spectra from above or higher intensity values. The BHS and modified BHS obtained using R1 as spectral reference are those shown in Figure 5. If we compare them to those in Figure 7, they are already an improvement considering the two smaller clusters close to the origin in

Figure 5(b). However, despite R1 being a better reference than 1-cardboard, it is still not an optimal one. This is because its shape is still highly similar to the ultramarine blue pigments that exist in the painting. The second way to achieve an optimum spectral reference is done by shifting the peaks of the spectrum to the left (shorter wavelength) or right (longer wavelength) directions. R2 in Figure 6(b) was generated by first mimicking the same ultramarine blue shape as R1 (sample #34 in Table 1), then shifting the spectrum to the right direction and finally multiplying its values by 0.5 such that R2 covers the four spectra of the pigments from below. The BHSs obtained by using R2 as a reference can be observed in Figure 8. Through the BHS, we can see that there are more than two clusters in the image. Then, as complementary information, the modified BHS provides the information that there is spectral variation that goes from red, lighter red, cardboard color, light blue, and then to darker blue, and this variation is shown in a continuous manner. This agrees with our initial visual observation of the image, that there are roughly four groups of pigments in the image. Furthermore, the BHSs also provide information that there are possibly regions in the image where the red pigment is applied in thin layers, such that they are transparent and their spectra is optically mixed with those of the cardboard.

To summarize, by considering the spectral set of our input image as a convex hull in the BHS or modified BHS spaces, the task of reference selection becomes easier and more practical. Knowing that the BHS axes are intensity and shape differences allows us to generate an artificial spectrum that will be located outside the initial convex hull, such that it becomes an optimum one. This can simply be carried out by taking any arbitrary spectrum from the initial set and further modifying it in both

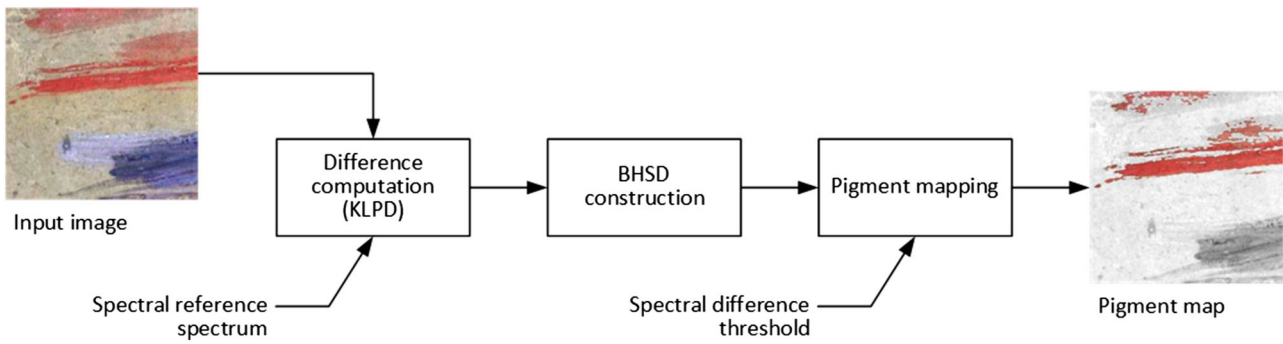


Figure 9. Pigment mapping workflow based on difference computation using KLPD measure and its representation using BHSD and modified BHSD.

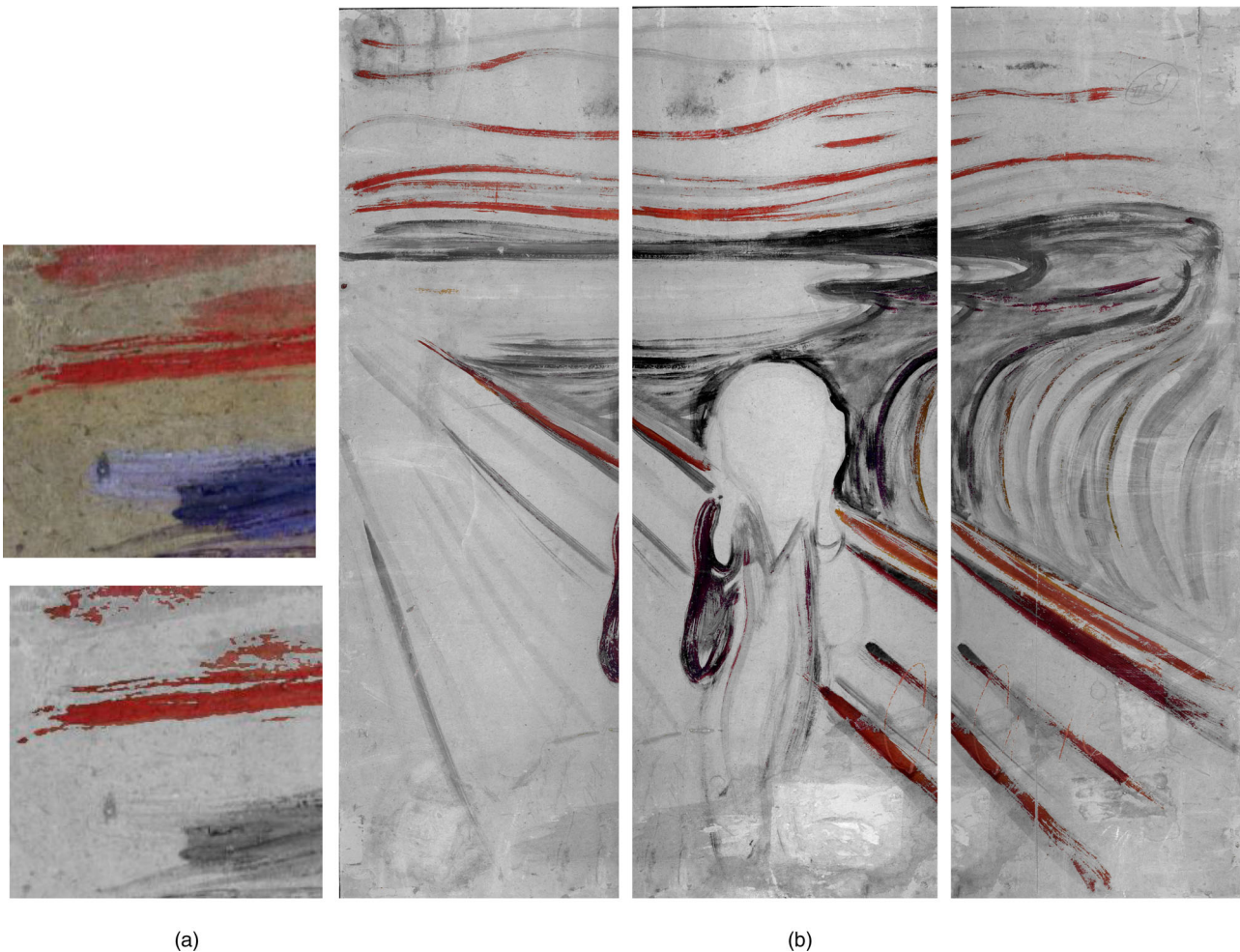


Figure 10. (a) Side-by-side comparison of a subset of the reverse side of *The Scream* and its vermilion map. (b) Vermilion maps for the whole surface of the reverse side of the painting. Note that in these maps, only pixels considered as containing vermilion are colored. The rest are represented in grayscale.

dimensions of the BHSD space, intensity and shape differences. Intensity modification is carried out through multiplication operation, such that the modified spectrum has an either higher or lower intensity than all other spectra in the initial set, in all the wavelengths or spectral

channels. Modification in the shape dimension can be carried out by shifting the spectrum to the direction of the shorter (left) or longer (right) wavelengths, keeping in mind that the resulting spectrum cannot already exist in the initial set. Illustrations and demonstrations in this

section have been provided by modifying an ultramarine blue sample from the painting, which was chosen merely for the purpose of the demonstration.

3.4. Discussion

In the classical similarity (or difference) based pigment discrimination task, typically the employed spectral difference function only measures differences in terms of shape, e.g., SAM and SCM. This widely accepted practice is based on the knowledge that the peaks and valleys of spectra belonging to identical pigments (or mixtures) will be located in nearly identical wavelengths. The variations in intensity are usually due to the lightness, opacity, or thickness of the paint layers. However, in this section, we have shown that intensity differences provide useful information for characterizing the distribution of pigment on a painting surface through bidimensional representations of spectral differences, i.e., BHSD and modified BHSD. They are enabled by the two independent components of the Kullback–Leibler pseudo-divergence (KLPD) measure. Inside the BHSD and modified BHSD representations, we can observe the spectral variations of a surface or object in a continuous manner. For example, we can observe the transition between pixels of pure vermilion and those of the cardboard in Figure 8. Moreover, we can derive that the in-between pixels are possibly vermilion pigments thinly applied on the cardboard, making the paint layer transparent.

In this section, we have also shown through Figures 5, 7 and 8, that the discrimination quality provided by a BHSD or its modified version is highly dependent on the chosen spectral reference. It is important to note that this is not a limitation of the representation. Rather, it should be regarded as the potential and flexibility of the representations. Experts in the cultural heritage

domain know the characteristics of materials they are interested in. For example, ultramarine blue pigment will have a reflectance peak at 500 nm. By using ultramarine blue as a spectral reference, they will be able to observe the distribution of vermilion pigments, since these pigments will be located far from the reference in the BHSD and modified BHSD.

Finally, the potential of KLPD and its representation in a BHSD and modified BHSD do not stop at the two-dimensional space. For the same object or surface under evaluation, several n spectral references can be employed, providing a representation or feature vector of size $2n$. Even if its visual representation will be limited to a three-dimensional space, by combining two shape and an intensity differences, this higher dimensional feature vector can be processed as classification or clustering tasks.

4. Pigment mapping

An immediate task that can be carried out using a spectral difference function and its representation in BHSD and modified BHSD is pigment mapping. The complete workflow that will be used in this section is as depicted by Figure 9. Using this workflow, the mapping of several pigments will be carried out for both sides of the case study painting, *The Scream* (1893).

4.1. Reverse side – Vermilion

Following the pigment mapping workflow in Figure 9, a vermilion map for a subset image of the reverse side of *The Scream* is obtained and shown Figure 10(a). To remind readers, this subset image is the same as what

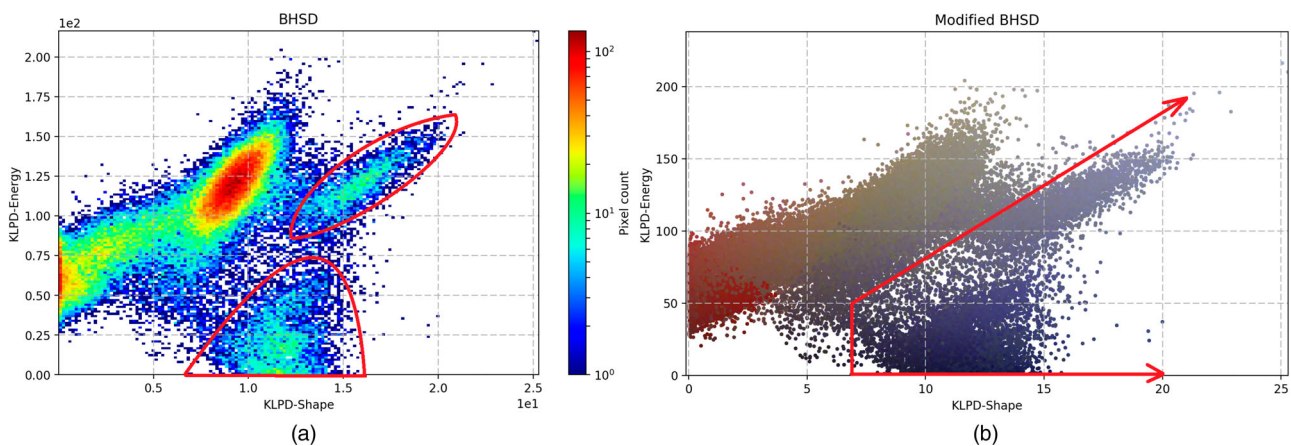


Figure 11. (a) BHSD and (b) modified BHSD of subset image shown in Figure 6(a), computed using a spectral reference that mimic the shape of sample #33 in Table 1, but of lower intensity values. Two clusters of ultramarine mixtures can be observed, they are manually circled in red in (a). Thresholds used for the mapping are shown in (b).

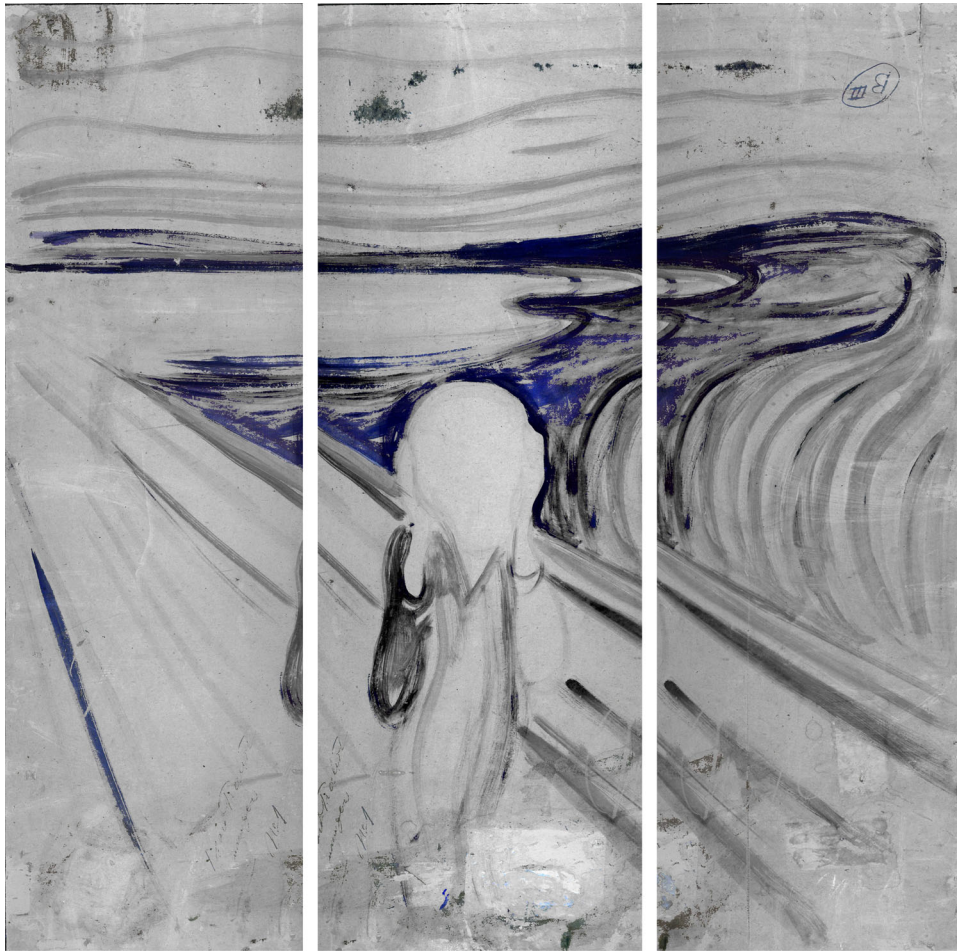


Figure 12. Maps for the mixture found in sample #34 in Table 1 (ultramarine blue, lead white, barites) for the reverse side of *The Scream* (1893). Only relevant pixels are colored, while the rest represented in grayscale.

has been used throughout Section 3 for illustrations and demonstrations of the representation and discrimination of spectral variation. The vermilion map (Figure 10(a), bottom) is obtained by choosing a threshold for the

BHSD representations that were shown in Figure 8. Pixels considered the vermilions are those located within shape threshold $T_G \geq 13$ and intensity threshold $10 \leq T_W \leq 150$ in the BHSDs.

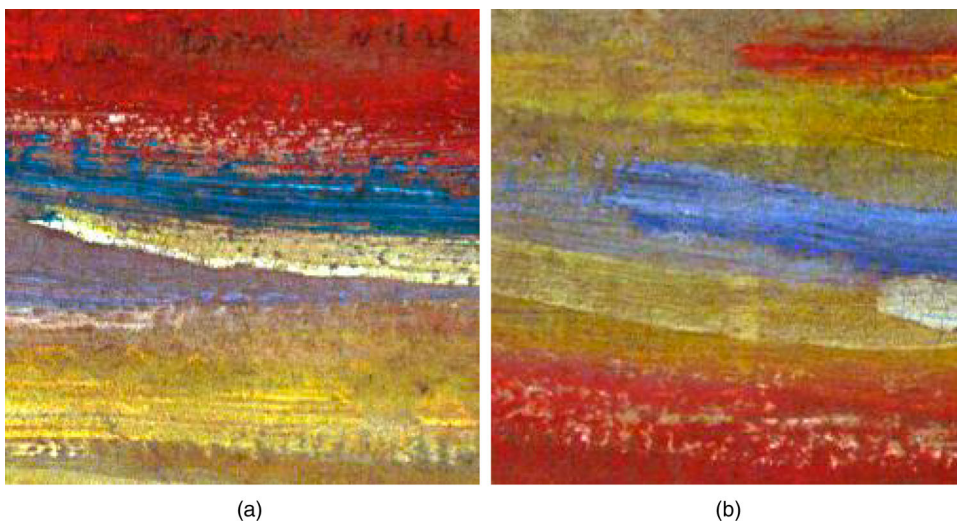


Figure 13. Two subsets of the front side of *The Scream* (1893). Both extracted from the leftmost cutout.

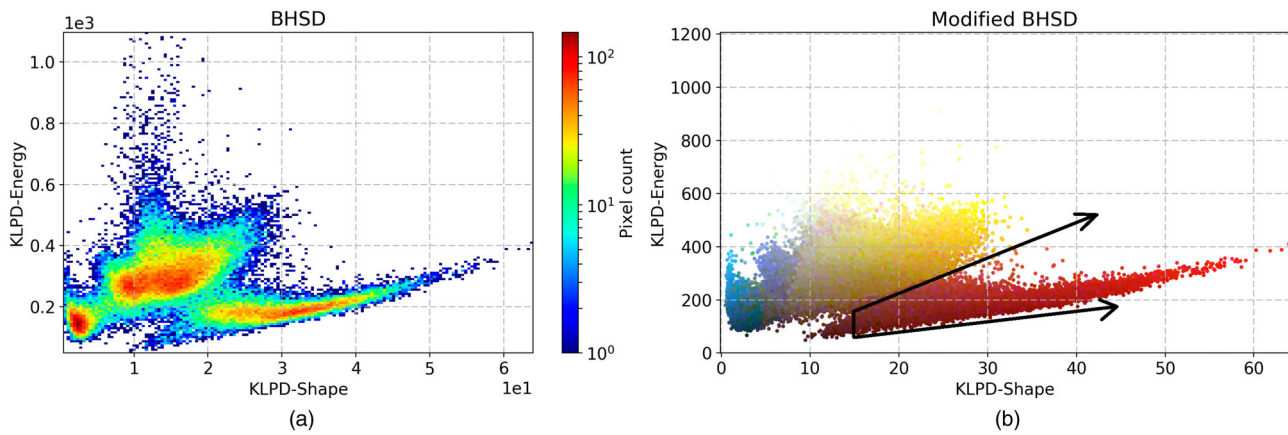


Figure 14. (a) BHS and (b) modified BHS of a subset image of the front side of *The Scream* (1893) shown in Figure 13(a). They are obtained using a spectral reference generated based on the spectrum of sample #20.

Using the same thresholds, the mapping is extended to the entire surface of reverse side of the painting. The results can be seen in Figure 10(b), where only pixels classified as vermilion are colored, while the rest are presented in grayscale. Note that these pixels are not always considered pure vermilion. They can also be considered as where traces of the pigment can be found, in thin layers or possibly mixed with relatively low amounts of other pigments.

4.2. Reverse side – mixed ultramarine blue

A mixture of ultramarine blue, lead white, and barites was found on the reverse side of the painting, see sample #34 in Table 1. In this section, we want to extend this point analysis result to the entire surface of this side of the painting using the same method as previously carried out for

vermilion. For this mixture, we can immediately apply thresholding to the representations in Figure 8. However, there, the distribution of this mixture is rather concentrated around the origin. This is understandable because the spectral reference was a slightly modified spectrum of this exact mixture. To have a better discrimination for it, we would rather choose another spectral reference that would push the distribution of the mixture away from the origin, such that we are able to observe and decide for a better threshold selection.

From the representation in Figure 8(b), we know that vermilion and the mixed ultramarine blue are located in both ends of the horizontal axis of modified BHS. Thus, if we are to choose a spectral reference that is mimicking the vermilion, we know we will have the vermilion distribution concentrated around the origin and the mixture will be located in the far end of the horizontal

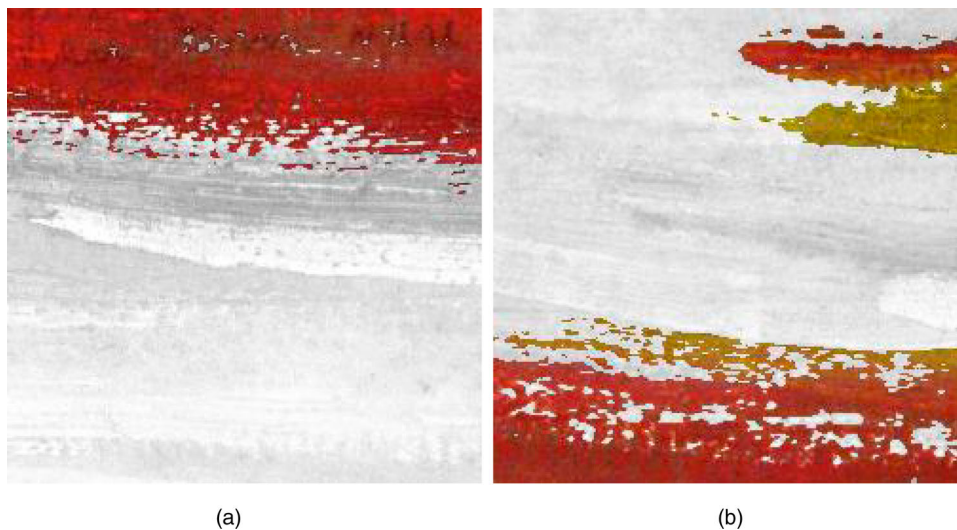


Fig. 15. Vermilion maps for two subsets of the front side of *The Scream* (1893) shown in Figure 13. The map in (a) demonstrate a relatively good classification of vermilion. However, the result in (b) shows also a misclassification for yellow pigments. Note that pixels represented in grayscale are not detected as vermilion.

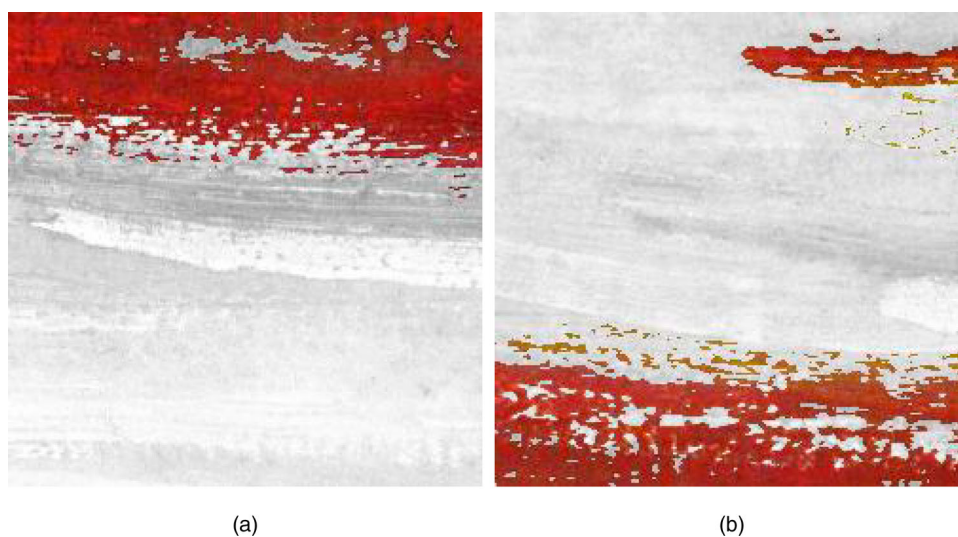


Figure 16. Vermilion maps for two subsets of the front side of *The Scream* (1893) previously shown in [Figure 13](#) after a second step of thresholding involving a second spectral reference. Pixels represented in grayscale are not detected as vermilion.

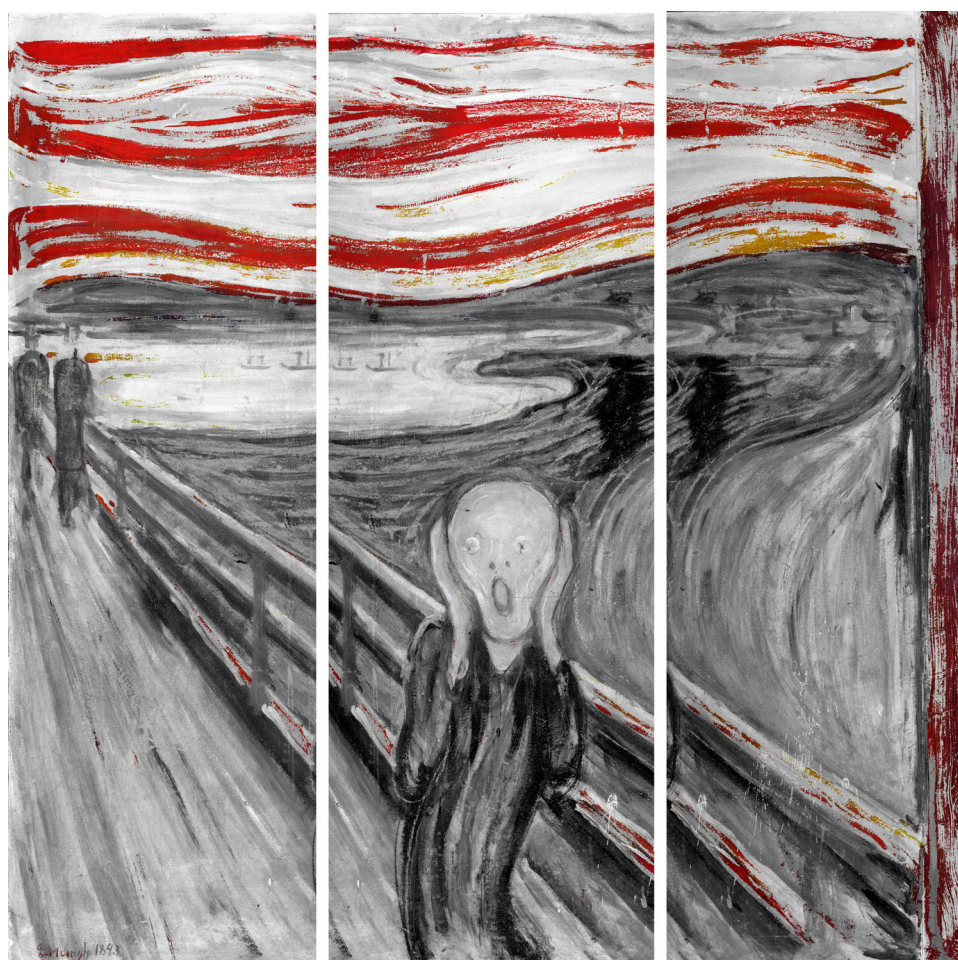


Figure 17. Maps for mixtures with vermilion for the whole surface of the front side of *The Scream* (1893). Only relevant pixels are colored, while the rest represented in grayscale. The yellow pixels are also detected as containing vermilion; they are possibly mixed with vermilion as the case of sample #14 in [Table 1](#).

axis. BHSDs shown [Figure 11](#) are obtained using a reference spectrum whose shape is of sample #33 in [Table 1](#), but of lower intensity values. From these representations, we can observe two clusters that belong to the mixtures of ultramarine blue, i.e., those that are within red circles in [Figure 11\(a\)](#). The obtained distribution allows us to empirically decide the thresholds for the mapping, see [Figure 11\(b\)](#). Finally, using these thresholds, maps for the pigment mixture of ultramarine blue, lead white, and barites are shown in [Figure 12](#).

4.3. Front side – Vermilion

Compared to the reverse side, pigment mapping of the front side of *The Scream* (1893) is expectedly more challenging. This is because in the reverse side, what is now considered as an unfinished version of *The Scream*, the brushstrokes are significantly less mixed. It is also under a better condition compared to the front side, which has been under exposure to light, dirt, weathering, etc. for decades. Due to this, pigment mapping of the front side is highly likely needing more than one spectral reference.

Before working for the entire front side of the painting, a subset is selected to illustrate the impact of reference selection and the challenge of mapping this particular painting, see [Figure 13\(a\)](#). In the subset, we can observe red, turquoise, and mixtures of whites and yellows. The red colors are possibly of similar mixture to sample #17 in [Table 1](#), likely vermilion and gypsum. Thus, we are interested in correctly detecting this red region of the subset as vermilion.

From vermilion mapping results of the reverse side of the painting (Section 4.1), we know that choosing an ultramarine blue-like spectral reference will allow pushing the distribution of vermilion-containing pixels away from the origin, in the direction of the horizontal axis ([Figure 8\(b\)](#)). However, we also know that the front side of the painting is highly mixed and deteriorated compared to the reverse side. Thus, if we are to generate an ultramarine spectral reference, it has to be one that mimics an ultramarine mixture that is found on the front side rather than the reverse side of the painting. Sample #20 in [Table 1](#) is found to be a mixture of artificial ultramarine blue with some other white pigments/colorants. A spectral reference is then generated based on the spectrum of this sample and the BHSDs of the subset image of interest can be observed in [Figure 14](#).

Using the thresholds as illustrated in [Figure 14\(b\)](#), vermilion maps for both subsets shown in [Figure 13](#) are obtained and provided in [Figure 15](#). Vermilion mapping for the first subset seems reasonable. Regions with turquoise, yellow, and other colors are not detected as

vermilion. However, in the second subset, we can observe that there exists several misclassification for the yellow colored pixels. While such results are understandable because there are yellow colors that are mixed with vermilion, such as in sample #14, the results can be improved by using another spectral reference that maximizes the difference between the red and yellow colored pixels. Then, by combining the shape differences from both references, new representations can be plotted. For brevity, here we skip the procedure and intermediate thresholding results. The final mapping for both subset images after combining results from the two references can be observed in [Figure 16](#). Finally, full vermilion maps for the front side of the painting are provided in [Figure 17](#).

4.4. Discussion

Pigment mapping is an immediate application of the bidimensional representations of spectral variation introduced in the previous section, BHSD and modified BHSD. By simply giving thresholds in the representation space, we can map the occurrence of pigments of interest in the entire surface of a painting. Moreover, in this section, we have applied pigment mapping for the reverse and front sides of *The Scream* (1893), for vermilion pigment and mixed ultramarine blue.

Mapping the reverse side of the painting is a relatively easier task than for the front side. This is because the reverse side can be considered as a sketch or layout, painted with confident and large brushstrokes, making the pigments on this side not as highly mixed as the front side. Moreover, it is also relatively well preserved and has not been exposed to dirt and weather as the front side of the painting. As a result, the pigment mapping for vermilion and mixture of ultramarine blue only required each a single BHSD processing with one spectral reference.

Pigment mapping task becomes more challenging as we tried to map vermilion on the front side of the painting. To tackle the deterioration issue of the front side, the spectral reference is chosen to mimic mixture of ultramarine blue that is found on this side rather than that of the reverse side. However, this does not solve the challenge posed by the highly mixed nature of the pigments. For this issue, two references have to be used in combination. After the first thresholding of BHSD obtained using the first reference, several yellow colored pixels were identified as vermilion. A second spectral reference was then selected to maximize the difference between vermilion and these yellow pixels. Finally, the processing in which this second reference was incorporated yielded a better mapping of vermilion.

Thresholding applied on the representation space can be considered as a classification approach. The limitation to such approach lies in the fact that it provides a binary decision, whether a certain pixel is vermilion or not, which evidently is not always relevant in cases where pigments are highly mixed. However, depending on the choice of the threshold, the user is allowed to determine how strict he or she wants the results to be. As the threshold becomes more narrow or strict, the mapped pigment becomes purer. On the other hand, when the threshold is set looser, the obtained map should be treated as indication of where this certain pigment occurs, be it pure or in mixture. Although it has to be noted, that the map is an indication of occurrence and does not provide information of pigment concentration.

Apart from its use in the task of pigment discrimination, BHSD and modified BHSD are generic representation spaces useful for the analysis and processing of hyperspectral images in any application domain. In a most recent study, this space was used to define statistics to measure the variability of hyperspectral texture images (Deborah, Richard, and Hardeberg 2018). By allowing observing, analyzing, and quantifying spectral variability in a reduced space, their potential lies in many different application fields. In the remote sensing field, the concept of spectral variability has been used to solve unmixing tasks (Drumetz, Chanussot, and Jutten 2016). It also remains to be explored how feature vectors computed in this space can be used in medical applications, such as dermatological diagnosis based on hyperspectral imaging (Koprowski et al. 2014).

5. Conclusion and future works

In this study, we have introduced a spectral-divergence based representation space for spectral variation, BHSD and modified BHSD. This representation is built based on Kullback-Leibler pseudo-divergence (KLPD) which has been shown in previous studies to be more accurate than other more commonly used similarity metrics. Note also that a prior study has demonstrated the direct relationship between BHSD representation and expert judgment on pigment discrimination. We have also illustrated and demonstrated the use of these BHSDs using *The Scream* (1893) by Edvard Munch as a case study. In addition to using *The Scream* (1893) for the demonstration of use for BHSD, we have provided several pigment mappings for both sides of this painting, vermilion and mixed ultramarine blue.

The use of BHSD and modified BHSD is not limited to pigment mapping task. By using multiple references, a feature vector of spectral differences for every pixel in

the image can be obtained. In such a higher dimensional space, a more complex classification task will become possible. It also opens the possibility to carry out pigment unmixing task, which will provide not only information of occurrence, but also an estimation of pigment concentration in any given pixel.

Notes

1. <https://www.rese-apps.com/software/glimps/free-enviimage-viewer.html>.
2. Metrology, as defined by the International Bureau of Weights and Measures (BIPM), is “the science of measurement, embracing both experimental and theoretical determination at any level of uncertainty in any field of science and technology,” taken from <https://www.bipm.org/en/worldwide-metrology/>. Accessed March 5, 2018.
3. By “true color,” we mean any color representation or space chosen by the user. It can be color simulated for the human visual system under D65 illuminant or color generated by some software using a certain optimization.

Disclosure statement

No potential conflict of interest was reported by the authors.

Notes on contributors

Hilda Deborah received her BSc and MSc degrees from the University of Indonesia in 2010 and Erasmus Mundus Color in Informatics and Media Technology (CIMET) in 2013, respectively. She obtained her PhD degree from a cotutelle arrangement between the Norwegian University of Science and Technology (NTNU) and University of Poitiers (France) in 2016. She is currently a Marie Curie Postdoctoral Fellow at NTNU and University of Iceland, working towards the development of a metrological framework for hyperspectral texture assessment and processing. Her research focus is within hyperspectral imaging and mathematical morphology, with an application focus in the field of cultural heritage and remote sensing. Address: Department of Computer Science, NTNU in Gjøvik, postboks 191, NO-2802 Gjøvik, Norway. Email: hilda.deborah@ntnu.no.

Sony George is currently Associate Professor at The Norwegian Colour and Visual Computing Laboratory, Norwegian University of Science and Technology (NTNU) since 2017. Before joining NTNU, he has worked as a researcher at Gjøvik University College, Norway. Sony obtained a PhD in Photonics from the Cochin University of Science and Technology, India in 2012. He has been involved in imaging research in various leading research centers in India and holds a number of international publications. His research interests are in the field of color imaging, spectral image processing, 3D imaging, etc. He has been involved in several national and EU projects in multiple roles: EU MSCA-ITN project HiPerNav (722068, as project manager), EU MSCA-ITN project CHANGE (813789, as deputy coordinator). He has been active member in the EU COST Actions TD1201 COSCH (Color and Space


in Cultural Heritage) and CA16101 MULTIFORESEE. Address: As for Deborah. Email: sony.george@ntnu.no.

Jon Y. Hardeberg received his sivilingeniør (MSc) degree in signal processing from the Norwegian Institute of Technology in Trondheim (Norway) in 1995, and his PhD from the École Nationale Supérieure des Télécommunications in Paris (France) in 1999. After a short but extremely valuable industry career near Seattle (USA), where he designed, implemented, and evaluated color imaging system solutions for multifunction peripherals and other imaging devices and systems, he returned to academia and Norway in 2001. He is currently Professor of color imaging at the Department of Computer Science at The Norwegian University of Science and Technology (NTNU). He is a member of the Norwegian Colour and Visual Computing Laboratory, where he teaches, supervises MSc and PhD students, and manages international study programs and research projects in the field of color imaging. He has co-authored more than 300 publications within the field. Address: As for Deborah. Email: jon.hardeberg@ntnu.no.

ORCID

Hilda Deborah  <http://orcid.org/0000-0003-3779-2569>

Sony George  <http://orcid.org/0000-0001-8436-3164>

Jon Yngve Hardeberg  <http://orcid.org/0000-0003-1150-2498>

References

- Almeida, P., C. Montagner, R. Jesus, N. Correia, M. Vilarigues, M. J. Melo, and S. Nascimento. 2013. "Analysis of Paintings Using Multi-Sensor Data." Signal Processing Conference (EUSIPCO), Proceedings of the 21st European. IEEE.
- Aslaksby, T. E. 2015. "Edvard Munch's Painting The Scream (1893): Notes on Technique, Materials and Condition." In *Public Paintings by Edvard Munch and His Contemporaries: Change and Conservation Challenges*, 52–71. London: Archetype Publications.
- Bacci, M., M. Picollo, G. Trumpy, M. Tsukada, and D. Kunzelman. 2007. "Non-Invasive Identification of White Pigments on 20th-century Oil Paintings by Using Fiber Optic Reflectance Spectroscopy." *Journal of the American Institute for Conservation* 46 (1): 27–37.
- Baronti, S., A. Casini, F. Lotti, and S. Porcinai. 1998. "Multispectral Imaging System for the Mapping of Pigments in Works of Art by Use of Principal-component Analysis." *Applied Optics* 37: 1299–1309.
- Cosentino, A. 2014. "Identification of Pigments by Multispectral Imaging: A Flowchart Method." *Heritage Science* 2 (8): 1–12. doi:10.1186/2050-7445-2-8.
- Daniel, F., A. Mounier, J. Pérez-Arantegui, C. Pardos, N. Prieto-Taboada, S. Fdez-Ortiz de Vallejuelo, and K. Castro. 2016. "Hyperspectral Imaging Applied to the Analysis of Goya Paintings in the Museum of Zaragoza (Spain)." *Microchemical Journal* 126: 113–120.
- Deborah, H. 2016. "PhD Thesis: Towards Spectral Mathematical Morphology." NTNU and University of Poitiers. <http://hdl.handle.net/11250/2433012>.
- Deborah, H., J. S. Ferrer, I. C. Sandu, S. George, and J. Y. Hardeberg. 2017. "Old Man in Warnemünde (1907) Colouring Palette: A Case Study on the Use of Hyperspectral Imaging for Pigment Identification." Color and Imaging Conference, 339–344. Society for Imaging Science and Technology.
- Deborah, H., S. George, and J. Y. Hardeberg. 2014. "Pigment Mapping of The Scream (1893) Based on Hyperspectral Imaging." International Conference on image and Signal processing, 247–256. Springer International Publishing.
- Deborah, H., N. Richard, and J. Y. Hardeberg. 2015. "A Comprehensive Evaluation of Spectral Distance Functions and Metrics for Hyperspectral Image Processing." *IEEE Journal of Selected Topics in Applied Earth Observations and Remote Sensing* 8 (6): 3224–3234.
- Deborah, H., N. Richard, and J. Y. Hardeberg. 2018. "Application of Spectral Statistics to Spectral Texture Discrimination." Colour and visual Computing Symposium, Gjøvik.
- de Carvalho, Jr., O. A., and P. R. Meneses. 2000. "Spectral Correlation Mapper (SCM): An Improvement on the Spectral Angle Mapper (SAM)." Summaries of the 9th JPL Airborne Earth Science Workshop 1, 65–74.
- Delaney, J. K., E. Walmsley, B. H. Berrie, and C. F. Fletcher. 2005. Multispectral Imaging of Paintings in the Infrared to Detect and Map Blue Pigments. In *Scientific Examination of Art — Modern Techniques in Conservation and Analysis*, 120–136. Washington, DC: The National Academies Press.
- Delaney, J. K., J. G. Zeibel, M. Thoury, R. Littleton, M. Palmer, K. M. Morales, and A. Hoenigswald. 2010. "Visible and Infrared Imaging Spectroscopy of Picasso's Harlequin Musician: Mapping and Identification of Artist Materials in Situ." *Applied Spectroscopy* 64 (6): 584–594.
- Drumetz, L., J. Chanussot, and C. Jutten. 2016. "Variability of the Endmembers in Spectral Unmixing: Recent Advances." Hyperspectral Image and Signal Processing: Evolution in Remote Sensing (Whispers), 8th Workshop, 1–5.
- Grabowski, B., W. Masarczyk, P. Głomb, and A. Mendys. 2018. "Automatic Pigment Identification from Hyperspectral Data." *Journal of Cultural Heritage* 31 (May–June): 1–12.
- Hardeberg, J. Y., S. George, F. Deger, I. Baarstad, and J. E. Palacios. 2015. "Spectral Scream: Hyperspectral Image Acquisition and Analysis of a Masterpiece." In *Public Paintings by Edvard Munch and His Contemporaries: Change and Conservation Challenges*, 72–83. London: Archetype Publications.
- Koprowski, R., S. Wilczyński, Z. Wróbel, S. Kasperczyk, and B. Błońska-Fajfrowska. 2014. "Automatic Method for the Dermatological Diagnosis of Selected Hand Skin Features in Hyperspectral Imaging." *BioMedical Engineering OnLine* 13: 1–15.
- Kruse, F., A. Lefkoff, J. Boardman, K. Heidebrecht, A. Shapiro, P. Barloon, and A. Goetz. 1993. "The Spectral Image Processing System (SIPS): Interactive Visualization and Analysis of Imaging Spectrometer Data." *Remote Sensing of Environment* 44 (2–3): 145–163.
- Mounier, A., C. Denoël, and F. Daniel. 2016. "Material Identification of Three French Medieval Illuminations of the XVIth Century by Hyperspectral Imaging (Treasury of Bordeaux Cathedral, France)." *Color Research and Application* 41: 302–307.
- Pelagotti, A., A. del Mastio, A. de Rosa, and A. Piva. 2008. "Multispectral Imaging of Paintings: A Way to Material Identification." *IEEE Signal Processing Magazine* 25 (4): 27–36.
- Plutino, A., N. Richard, H. Deborah, C. Fernandez-Maloigne, and N. G. Ludwig. 2017. "Spectral Divergence for Cultural

- Heritage Applications.” Color and imaging Conference, 141–146. Society for Imaging Science and Technology.
- Richard, N., D. Helbert, C. Olivier, and M. Tamisier. 2016. Pseudo-divergence and Bidimensional Histogram of Spectral Differences for Hyperspectral Image Processing. *Journal of Imaging Science and Technology*, 60(5), 50402-1–50402-13.
- Rohani, N., J. Salvant, S. Bahaadini, O. M. W. Cossairt, and A. Katsaggelos. 2016. “Automatic Pigment Identification on Roman Egyptian Paintings by Using Sparse Modeling of Hyperspectral Images.” 24th European Signal Processing Conference (EUSIPCO), 2111–2115. Budapest, Hungary.
- Savitzky, A., and M. J. Golay. 1964. “Smoothing and Differentiation of Data by Simplified Least Squares Procedures.” *Analytical Chemistry* 36 (8): 1627–1639.
- Singer, B., T. E. Aslaksby, B. Topalova-Casadiago, and E. S. Tveit. 2010. “Investigation of Materials Used by Edvard Munch.” *Studies in Conservation* 55: 274–292.
- Zhao, Y. 2008. “PhD Thesis: Image Segmentation and Pigment Mapping of Cultural Heritage Based on Spectral Imaging.” Rochester Institute of Technology.

Appendix 1. Comparison to SAM and SCM

In an earlier case study, we have compared the performance of spectral angle mapper (SAM) and spectral correlation mapper (SCM) for mapping the pigments of the front side of *The Scream* (1893) (Deborah, George, and Hardeberg 2014). In

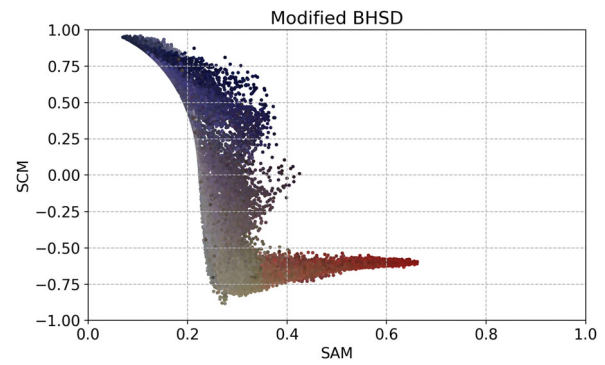


Figure A1. Modified BHS D for subset image shown in Figure 6 (a), obtained through using SAM and SCM as the X- and Y-axes, respectively. Note that the range of values obtained by SAM and SCM are $[0, 1]$ and $[-1, 1]$, respectively. Results obtained the aforementioned parameters for SAM and SCM can be observed in Figure A2, with original image and KLPD result also provided for comparison. In addition to the reddish pigments that are highly likely vermilion, SAM also detects purplish colors located at the arm of the figure at the center of the painting as vermilion. For the same region, SCM does not deem it as vermilion. The problem with SCM, however, lies in its false detection of cardboard regions as vermilion. KLPD also detects some part of the arm of the figure as vermilion, but not as severe as the case of SAM. In addition, KLPD does not consider the cardboard regions as containing vermilion.

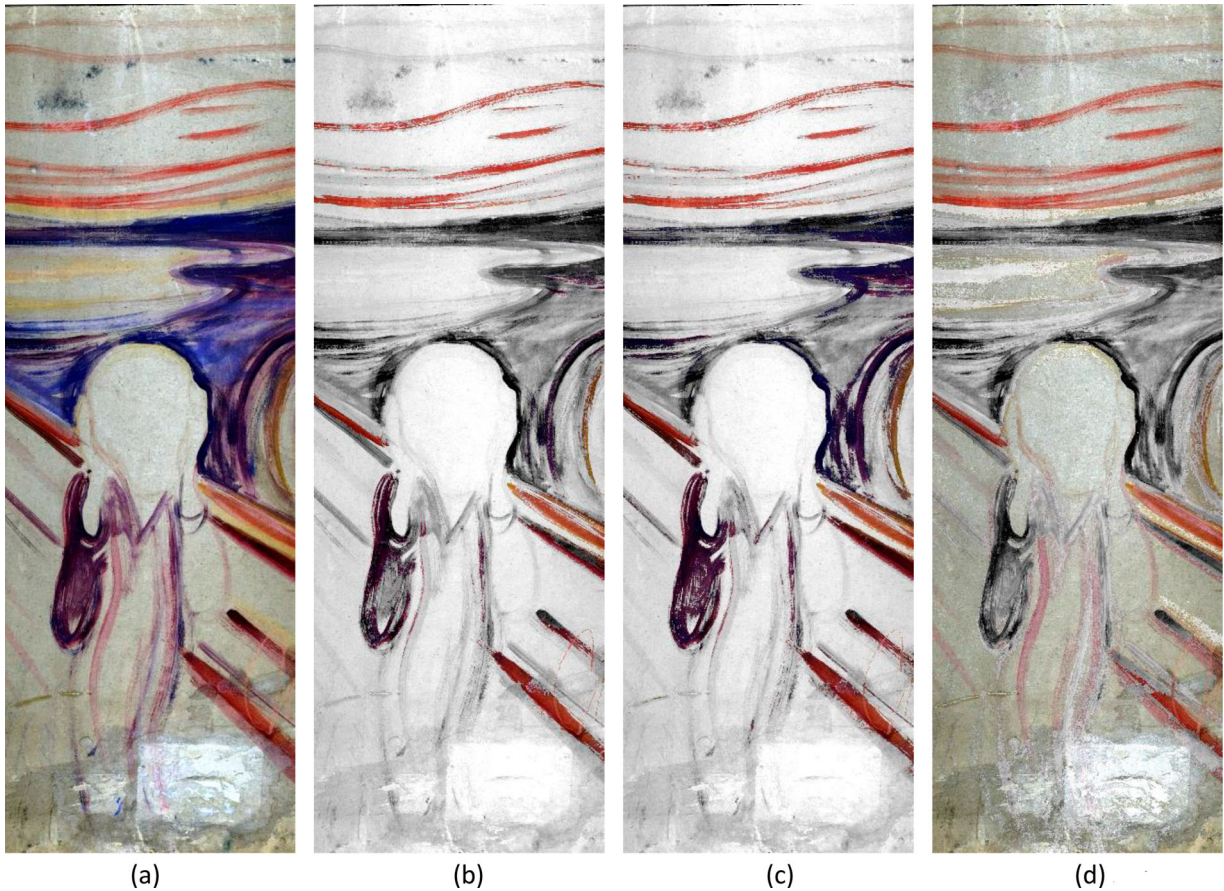


Figure A2. Original image of one cutout of the reverse side of *The Scream* (1893) and its mapping results for vermilion pigment, obtained by KLPD, SAM, and SCM. Note that only pixels detected as vermilion are colored, the rest remains in grayscale.

it, it had been shown that cases of erroneous identification and mapping resulting from SAM were indeed improved by SCM. Nevertheless, results obtained by SAM and SCM for vermilion pigment on one cutout of the reverse side of the painting are provided and contrasted to that of KLPD in the following. They use the same spectral reference as that of KLPD, i.e., R2 shown in [Figure 6\(b\)](#). Then, their thresholds are set with $T_{\text{SAM}} \geq 0.4$ and $0.5 \leq T_{\text{SCM}} \leq 0.75$. The choice of these

thresholds are made through observing the modified BHSD obtained for a subset image ([Figure 6a](#)) that is provided in [Figure A1](#). In this BHSD, the two axes are both representing shape differences, albeit representing different similarity functions. As a final note, despite providing a BHSD that combines the result of SAM and SCM in a single visualization, the processing of the results do not combine the two since the aim is to compare their individual performances against KLPD.